Journal of Controlled Release 337 (2021) 407–416

Contents lists available at ScienceDirect

Journal of Controlled Release

journal homepage: www.elsevier.com/locate/jconrel

Multiscale pharmacokinetic modeling of systemic exposure of subcutaneously injected biotherapeutics

Fudan Zheng, Peng Hou, Clairissa D. Corpstein, Kinam Park, Tonglei Li *

Industrial & Physical Pharmacy, Purdue University West Lafayette, Indiana, USA

ARTICLE INFO

Keywords:
mAb
Simulation
Subcutaneous absorption
Biotherapeutics
Physiologically-based pharmacokinetics
Multiscale modeling
Bioavailability

ABSTRACT

Subcutaneously injected formulations have been developed for many biological products including monoclonal antibodies (mAbs). A knowledge gap nonetheless remains regarding the absorption and catabolism mechanisms and kinetics of a large molecule at the administration site. A multiscale pharmacokinetic (PK) model was thus developed by coupling multiphysics simulations of subcutaneous (SC) absorption kinetics with whole-body pharmacokinetic (PK) modeling, bridged by consideration of the presystemic clearance by the initial lymph. Our local absorption simulation of SC-injected albumin enabled the estimation of its presystemic clearance and led to the whole-body PK modeling of systemic exposure. The local absorption rate of albumin was found to be influential on the PK profile. Additionally, nineteen mAbs were explored via this multiscale simulation and modeling framework. The computational results suggest that stability propensities of the mAbs are correlated with the presystemic clearance, and electrostatic charges in the complementarity-determining region influence the local absorption rate. Still, this study underscores a critical need to experimentally determine various biophysical characteristics of a large molecule and the biomechanical properties of human skin tissues.

1. Introduction

The advent of recombinant DNA and hybridoma technologies has spurred the development of biotherapeutic products that demonstrate remarkable targeting specificity and treatment potency [1,2]. There are more than 200 protein products on the market and at least half are monoclonal antibodies (mAbs) [3]. In addition to intravenous (IV) injection, subcutaneous (SC) delivery has become a favorable route for administrating macromolecules. One third of the approved mAbs in the last decade are given via SC injection, mostly driven by the need for self-administration to improve patient compliance and reduce treatment burden [4,5]. Moreover, because of the extended absorption kinetics, a locally injected drug enables added benefits of sustainable release and prolonged systemic exposure, desired for treating chronic diseases [6]. Notwithstanding these advantages, there is a substantial knowledge gap in the mechanistic understanding of SC transport and absorption kinetics of a protein product, limiting the translation into clinic [7].

Upon injection, biotherapeutic molecules diffuse into the interstitial space of the subcutis and traverse through dense extracellular matrix (ECM) before permeating into the circulating vascular and or lymphatic vessels [8]. Diffusion of large molecules may be promoted by convective flow of interstitial fluid flow between blood vessels and lymphatic capillaries [9,10]. Most therapeutic macromolecules are heavier than 16 kDa and are expected to primarily enter lymphatic capillaries, which, compared with blood vasculatures, are more permeable due to the lack of steady basement membrane and tight junctions [11,12]. Still, vascular uptake of erythropoietin and leptin was observed to some extent in cannulated sheep models [13,14]; recent rat studies of cetuximab and trastuzumab also suggest such possibilities [15,16]. In addition to molecular size that limits the local absorption rate of a biomolecule, charge, molecular shape, and other biophysical properties are also regarded as influential [17–19], but mechanistic understanding of the in vivo fate remains limited [20,21].

Many injectable biopharmaceutics are of high concentration, likely susceptible to aggregation in the interstitium [22]. In addition, a protein molecule may further undergo intracellular proteolysis in lysosomes – a process called “first-pass catabolism” – after it is subjected to pinocytosis by endothelial cells through systemic circulation [23]. For a mAb,

Abbreviations: PK, pharmacokinetic; SC, subcutaneous; mPBPK, minimal physiologically-based pharmacokinetic; mAbs, monoclonal antibodies; ECM, extracellular matrix; FcRn, neonatal Fc receptor; TMDD, target-mediated drug disposition; NMSE, normalized mean squared error; CDR, complementarity-determining region..

* Corresponding author at: 525 Stadium Mall Dr., RHPH BuildingWest Lafayette, IN 47907, USA.
E-mail address: tonglei@purdue.edu (T. Li).

https://doi.org/10.1016/j.jconrel.2021.07.043
Received 31 March 2021; Received in revised form 19 June 2021; Accepted 24 July 2021
Available online 27 July 2021

recycling by the neonatal Fc receptor (FcRn) is known to mitigate the lysosomal degradation and thus affect its circulating half-life [24]. Proteolytic enzymes and migrating dendritic cells in tissues and lymph can also break down a biopharmaceutical molecule [25]. Studies in sheep with lymphatic cannulation suggest that protein degradation mainly occurs during passage through the lymphatics, prior to entering systemic circulation via the thoracic duct [26,27]. As such, the bioavailability of an injected biotherapeutic drug can range from 20% to 100% in humans [18,26]. Due to the intertwined influence by local and systemic disposition and clearance kinetics, it has been futile to directly scale the PK and bioavailability of locally injected biomolecules from animal models to humans [28]. In the absence of a mechanistic understanding and in silico models that capture the local absorption and presystemic catabolism, prediction of the systemic exposure of injectable biopharmaceuticals remains to be an unmet challenge for drug development [29,30].

Herein, we report a multiscale modeling approach to predict the systemic exposure of proteins and mAbs that are injected subcutaneously. The modeling framework integrates a multiphysics simulation of drug transport and absorption at the injection site with whole-body PK modeling of systemic biodistribution. The local simulation was developed by treating the subcutis as a homogenous, poroelastic media, and computing the mass transport of an injected drug under the influence of interstitial hydrodynamics, tissue deformation, and lymphatic absorption [31,32]. As first principles are utilized in the local simulation, drug transport and absorption in the SC tissue are governed by the physical properties of the drug, as well as by the physiological and anatomic attributes of SC tissue. A PBPK (physiologically-based pharmacokinetic) model – minimal PBPK (mPBPK) – was adopted to evaluate the systemic disposition and clearance of the absorbed drug from SC tissue. As it is true for most PK and PBPK modeling, kinetic parameters of a drug have to be data-fitted against pre- and clinical PK profiles. In our mPBPK, the parameters of a protein were obtained by fitting the plasma concentration data of IV injection available in the literature. Importantly, the presystemic clearance by initial lymphatics was further modeled in order to bridge the local simulation and systemic PK modeling.

In this report, we will firstly explain the overall simulation and modeling approach and then discuss computed results of albumin and the other nineteen mAbs. For the SC injected albumin, we were able to estimate its presystemic clearance in the initial lymphatics and systemic exposure from high-fidelity simulation of local absorption. For other mAbs, because of the lack of reliable physical properties to predict their local absorption kinetics and clearance parameters to compute the presystemic clearance, we conducted simulation experiments with the multiscale framework using assumptions of these properties to explore potential molecular factors that may impact the bioavailability of mAbs. The results support the feasibility of integrating multiphysics simulation of local absorption with whole-body PK modeling of systemic exposure.

2. Methodology

2.1. Simulation of local absorption from injection site

A multiphysics, spatiotemporal simulation model of drug transport and absorption of SC injection was previously developed by our group [31,32]. In this model, SC tissue is treated as a homogenous, poroelastic media (Fig. 1), in which hydrodynamics of the interstitial fluid is evaluated according to the poroelasticity [33] and Darcy's law [34]. Mass transport of drug molecules is described by the general convection-diffusion equation as follows:

$$\frac{\partial(\phi c_{sc})}{\partial t} + \nabla\cdot\left(-D_{eff}\nabla c_{sc}\right) + \nabla(\vec{v}\cdot c_{sc}) = -P_a c_{sc}\frac{S_{ly}}{V} \quad (1)$$

The terms on the left side of Eq. 1 represent mass accumulation, and diffusive and convective transport, respectively. ϕ is tissue porosity; c_{sc} is the drug concentration in the SC tissue; D_{eff} is the effective diffusion coefficient of the drug in tissue; $\vec{v}$ is the interstitial flow velocity. The right side of Eq. 1 represents the drug uptake rate by lymphatic vessels

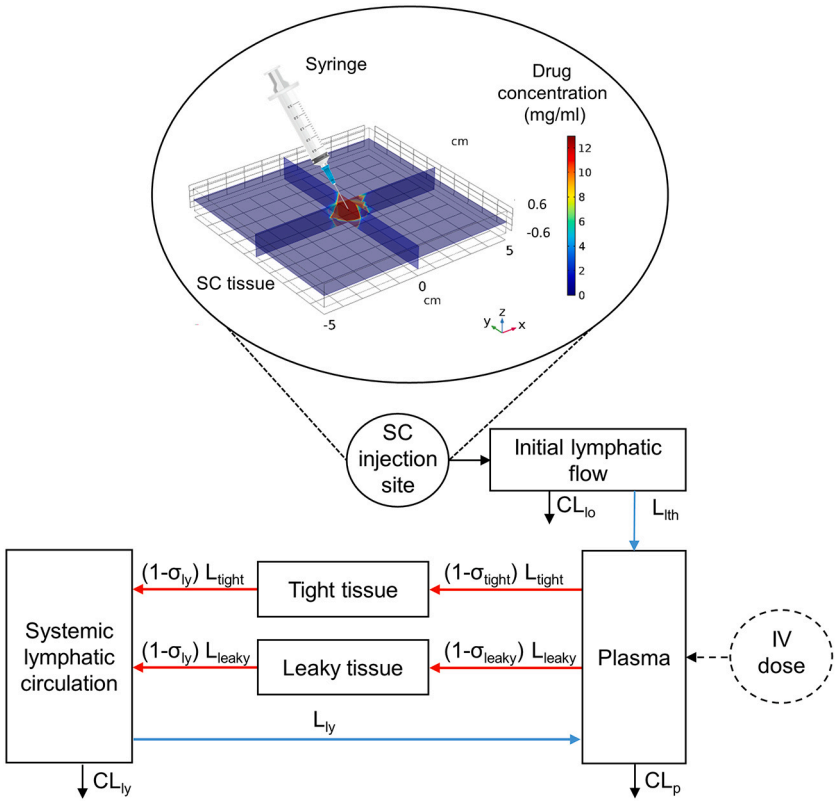

Fig. 1. Schematic of integrated SC injection site model with minimal PBPK model.

[35]. P_a is the apparent permeability of the drug across the lymphatic membrane. $\frac{S_{ly}}{V}$ is the surface area of lymphatic vasculatures per unit tissue volume. Vasculature absorption of large biomolecules is generally considered trivial from the injection site and thus ignored in this study; it can be, however, included with a similar term in Eq. 1 to that of lymphatic uptake (given that the respective parameters are available for the molecule of interest). In addition, transport of the interstitial fluid and deformation of the SC tissue are described by the respective equations. By numerically solving these equations with inputs of physical properties of drug and tissue attributes, the spatiotemporal distribution of the drug concentration, along with other physical quantities, can be calculated.

The overall absorption rate of a drug from the lymphatic capillaries at the SC injection site can then be obtained by integrating over the entire model domain of the porous medium:

$$m_{abs} = -\iiint_D \phi c_{sc} dV \tag{2}$$

$$k_{abs} = \frac{dm_{abs}}{dt} \tag{3}$$

where m_{abs} is the absorbed drug amount and k_{abs} is the local absorption rate. V and t stand for the tissue volume and time correspondingly. The absorption rate is further fitted by an exponential function of time ($m_{mAb} = Dose \cdot e^{a \cdot t}$) to be integrated into the mPBPK model.

2.2. Integration with mPBPK model

Disposition of the absorbed drug from the injection site to the systemic circulation is modeled with an mPBPK approach [25,36], schematically illustrated in Fig. 1. The amount of absorbed drug molecules that return to the injection site is assumed marginal and thus ignored in the model. This allows one-way coupling from the local simulation to the systemic PK model. The lymphatic system in humans from the perspective of local drug delivery is treated as an integration of two distinct (local and systemic) compartments [15]. Anatomically, initial lymph is collected by cannulation from the injection site, entering the systemic circulation of blood and lymph. The local lymph compartment thus bridges the local absorption simulation with the mPBPK model (Fig. 1); it considers the drug transport from the injection site through lymphatic trunks, lymph nodes, and the thoracic lymph duct before reaching the systematic circulation [26]. Presystemic degradation is assumed to mainly occur during the initial lymphatic flow, as suggested by studies with lymph-cannulated sheep models [26,37–41]. Protein catabolism at the injection site could be possible [40,41], but due to limited experimental data, it is omitted in our first-principle simulation model of local transport and absorption [31,32].

In mPBPK, tissues are classified into two collective compartments – tight and leaky tissues – in light of permeabilities through the capillary endothelium in tissues by macromolecules. The two compartments are looped with plasma and lymph flow, mimicking the anatomical organization. Brain, skin, adipose, and muscle tissues are lumped into tight tissue, whereas the rest is summed into leaky tissue, differentiated by the respective vascular reflection coefficients (σ_{tight} and σ_{leaky}) [42]. Reflection coefficient defines the percent of drug molecules at any given moment that fail to permeate through the capillary membrane of blood or lymphatic vessels. It represents flow resistance across a membrane and is thought to be, at least partially, determined by the relative size of drug molecules versus membrane pores [43]. The difference in extravascular distribution is commensurate with the understanding of disposition of macromolecules that are driven by interstitial fluid flow and lymphatic drainage [36]. At the systemic level, the transport kinetics based on mass balance of an administered drug is described by the following equations:

$$\frac{dc_{lo}}{dt} = \frac{1}{V_{lo}}(k_{abs} - c_{lo}L_{lth} - c_{lo}CL_{lo}) \tag{4}$$

$$\frac{dc_p}{dt} = \frac{1}{V_p}\left[c_{lo}L_{lth} + c_{ly}L_{ly} - c_pL_{tight}(1-\sigma_{tight}) - c_pL_{leaky}(1-\sigma_{leaky}) - c_pCL_p\right] \tag{5}$$

$$\frac{dc_{ly}}{dt} = \frac{1}{V_{ly}}\left[c_{tight}L_{tight}(1-\sigma_{ly}) + c_{leaky}L_{leaky}(1-\sigma_{ly}) - c_{ly}L_{ly} - c_{ly}CL_{ly}\right] \tag{6}$$

$$\frac{dc_{tight}}{dt} = \frac{1}{V_{tight}}\left[c_pL_{tight}(1-\sigma_{tight}) - c_{tight}L_{tight}(1-\sigma_{ly})\right] \tag{7}$$

$$\frac{dc_{leaky}}{dt} = \frac{1}{V_{leaky}}\left[c_pL_{leaky}(1-\sigma_{leaky}) - c_{leaky}L_{leaky}(1-\sigma_{ly})\right] \tag{8}$$

where, correspondingly, c_{lo}, c_p, c_{ly}, c_{tight}, and c_{leaky} are drug concentrations in the initial lymph, plasma, systemic lymph, interstitial spaces in the tight tissues and leaky tissues; V_{lo}, V_p and V_{ly} are volumes of initial lymph, plasma, systemic lymph; V_{tight} and V_{leaky} are the accessible spaces for drug to be distributed in the interstitial space of tight tissue and leaky tissues ($V_{tight} = 0.67V_{ISF} \bullet K_p$; $V_{leaky} = 0.33V_{ISF} \bullet K_p$; where K_p is volume fraction of drug distribution in the interstitium) [36,44]. L_{lth}, L_{ly}, L_{tight}, and L_{leaky} are respective lymphatic flow rates pertinent to the thoracic duct, systemic lymph, tight tissue, and leaky tissue. CL_{lo}, CL_{ly}, and CL_p represent drug clearances in the initial lymph, systemic lymph, and plasma; σ_{ly}, σ_{tight} and σ_{leaky} are reflection coefficients of drug molecule in the systemic lymph, and vascular capillary in tight and leaky tissues, respectively.

2.3. Simulation approaches and input parameters

Human serum albumin was chosen as a model drug in this study, given that its properties relevant to both local absorption and systemic circulation are available in the literature. Additionally, nineteen IgG-type mAb drugs either in late phase development or stages of approval were selected, largely due to availability of their IV and SC PK data in healthy volunteers or equivalent patient populations in the literature. In curating the PK data, injection doses considered for modeling were known to not induce target-mediated drug disposition (TMDD); those coadminsitered with hyaluronidase were excluded.

The physiologically-relevant PK parameters, including tissue volume and flow rate, were obtained from the literature and listed in Table 1 [25,44–48]. The lymph volume of the initial or presystemic flow summarized over the volumes of lymphatic capillaries, lymphatic trunk, node, and thoracic duct [25]. The systemic lymphatic reflection coefficient, σ_{ly}, was assigned as 0.2, according to the preceding papers of mAb PBPK models [36,49,50]. A small value represents little resistance of drug molecules to pass through lymphatic membrane; the literature adoption of 0.2 seems to be empirically assumed and warrants future experimental scrutiny. The plasma concentrations of IV and SC

Table 1
Physiological parameters used in the mPBPK model (70-kg adult).

Parameter	Value	Reference
Volume of distribution (L)		[25]
Initial lymphatics V_{lo}	0.0224	[25,45]
Systemic lymphatics V_{ly}	6.9576	[45]
Interstitial fluid V_{ISF}	8.8200	
Flow rate (L/h)		[46,47]
Thoracic duct L_{lth}	0.060	[48]
Systemic lymphatics L_{ly}	0.121	[44]
Tight tissue L_{tight}	0.040	[44]
Leaky tissue L_{leaky}	0.081	
Reflection coefficient		[42]
Systemic lymphatics σ_{ly}	0.2	

administration of albumin and therapeutic mAbs were extracted from the literature using Origin 8 (OriginLab Corporation, MA). Their respective bioavailability values were estimated using trapezoidal numerical integration in Matlab (R2018a, MathWorks Inc., MA). Drug specific parameters, including dose and formulation concentration, are listed in Table 2. V_p of each drug was calculated from the initial plasma concentration and dose; K_p was measured by using radiolabeled IgG isotypes and albumin to quantify the drug accessible distribution fraction in the interstitial fluid space [51–53]. Due to the sparse data available for mAbs, each mAb was assigned with a respectively measured K_p value according to the isotype of IgG (i.e., IgG_1: 0.695, IgG_2:0.436, IgG_4: 0.420) [51,52]; albumin was assigned with 0.665 [53].

The drug-specific mPBPK parameters, namely σ_{tight}, σ_{leaky}, CL_{ly}, and CL_p, were estimated by fitting the model against the IV data of plasma concentration-time profile of respective drugs using a nonlinear least-squares approach in Simbiology (Matlab R2018a). Fitting with single systemic clearance (CL_{ly}) was found to be capable of capturing the PK data of the twenty macromolecules investigated in this study. CL_p was thus set as zero. These PBPK parameters were employed in modeling the systemic exposure of SC administration of the corresponding drugs.

As aforementioned, the initial lymph compartment bridges the local simulation of drug transport and absorption at the injection site with the mPBPK model (Fig. 1). While the systemic PK parameters of a drug may be readily derived from clinical data of its IV administration, the drug-specific parameter of the initial lymph compartment, CL_{lo}, is not available when the drug is SC injected. It was thus a focus of this study to estimate this parameter by considering the simulated absorption rate from the injection site and the clinical data of an SC injected drug. This was completed for albumin, but for other mAbs, this could not be possible without making approximations.

Due to the limited availability of the physicochemical properties of the mAbs, drug absorption kinetics in the SC tissue could not be simulated. Still, two extreme scenarios were simulated to explore the possible kinetics of local absorption and CL_{lo} for each mAb. In the first case, the local absorption rate of each mAb was assumed to be the same as that of IgG, which was successfully simulated [31,32]. CL_{lo} of each mAb could then be derived. In the second case, the presystemic clearance of a mAb was assumed to be equivalent to its systemic clearance. The local absorption kinetics of each mAb could be approximated by fitting the simulated plasma concentration profile against the observed SC PK data. The estimated local absorption kinetics and CL_{lo} among nineteen mAbs were compared at a 50-mg dose. For the mAbs without clinically measured SC PK data at this dose, experimental data using the closest dose was extrapolated linearly to estimate the 50-mg PK profile.

To evaluate the goodness of fit between the simulated and observed PK data, the normalized mean squared error (NMSE) was calculated for each simulation as below:

$$NMSE = \frac{\sum_{i=1}^{n}\left(\widehat{C_{p_i}} - C_{p_i}\right)^2}{\sum_{i=1}^{n}\left(C_{p_i} - \overline{C_p}\right)^2} \quad (9)$$

where the subscript i refers to the respective plasma concentration at the ith out of n time points. $NMSE$ of zero indicates the perfect fit and a larger value is associated with a poorer fit between the simulated and observed data.

Table 2
Input parameters and characteristics of albumin and mAb used in simulation. V_p is plasma volume.

Drug	Isotype	IV dose (mg)	V_p (L)	SC concentration (mg/ml)	References
Albumin		1	3.1053	10	[54]
Adalimumab	IgG_1	89.69	2.8067	50	[55]
Anifrolumab	IgG_1	300	3.7063	150	[56]
Belimumab	IgG_1	240	2.9657	200	[57]
Brodalumab	IgG_2	210	3.3759	140	[58]
Canakinumab	IgG_1	600	3.1997	150	[59]
Daclizumab	IgG_1	200, 400	4.5892	150	[60]
Denosumab	IgG_2	70	2.8971	70	[61]
Dupilumab	IgG_4	79.5, 238.5, 636	2.5848	50	[62]
Emicizumab	IgG_4	14.68	2.9041	150	[63]
Erenumab	IgG_2	140	3.2270	70	[64]
Golimumab	IgG_1	100	3.4850	100	[65]
Guselkumab	IgG_1	2.04, 8.69, 21.27, 82.1, 240, 807	3.5358	100	[66]
Mepolizumab	IgG_1	250	2.3732	104	[67–69]
Risankizumab	IgG_1	200, 600	3.0498	90	[70]
Romosozumab	IgG_2	70, 350	2.7869	90	[71]
Sirukumab	IgG_1	23.61, 75.10, 207.90	3.6472	50	[72,73]
Tildrakizumab	IgG_1	33.78, 208.59	2.7111	100	[74]
Tocilizumab	IgG_1	81, 162	3.6206	180	[75]
Tralokinumab	IgG_4	150	2.7891	150	[76]

2.4. Analysis of model parameters with drug properties

It was the intention of this study to explore possible correlations between the estimated CL_{lo} and local absorption rate coefficient of therapeutic mAbs with formulation-relevant properties and certain molecular attributes of the corresponding drugs. The Pearson's correlation coefficient (r) between the CL_{lo} or absorption rate constant with these properties was assessed accordingly.

The formulation-relevant properties included drug concentration in the SC formulation and formulation pH, which were obtained from the package insert or product patents. Amino acid sequences of mAbs were obtained from the Therapeutic Antibody Database [77]. The sequences were used to calculate the charge-related parameters, aggregation tendency and complementarity-determining region (CDR) properties of the mAbs. Specifically, the isoelectronic point (pI) was estimated based on the average output of ExPASy-ProParam [78] and Protein Calculator v3.4 [79]. The absolute difference between pI and physiological pH 7.4 was thereby calculated. Protein Calculator was also used to compute the molecular charge at pH 7.4 and at the formulation pH. The scaled solubilities were estimated using Protein-Sol [80]. The total hot-spot area of aggregation was evaluated by Aggrescan [81]. The aggregation propensity of beta-sheets in heavy chains and light chains was computed using the Tango algorithm [82]. Metrics of CDR, including the surface hydrophobicity, positive charge, negative charge in the CDRs, and charge symmetry in the variable region, were obtained from SAbPred-TAP [83]. Additional biophysical properties of these mAbs measured by constructing isotype-matched IgG_1 antibodies were collected from the literature (excluding Emicizumab, Erenumab, and Risankizumab) [84].

3. Results and discussion

3.1. Systemic PK modeling

The mPBPK model (Fig. 1) was employed to compute IV plasma profiles of albumin and nineteen mAbs which were fitted against respective clinical data. Drug-dependent parameters, including σ_{tight}, σ_{leaky}, and CL_{ly}, were derived from the data fitting. The previously developed mPBPK model assumed V_p as being drug-independent [36], making it difficult in capturing the initial phase of the PK profile. V_p was allowed in this study as an adjustable parameter for albumin and

nineteen mAbs. The average value is 3.17 with the standard deviation of 0.50 L. This agrees with the human plasma volume and the reported volume of the central compartment in the two-compartment PK model commonly used for mAbs [45,85]. Table 3 lists the estimated parameters derived with the mPBPK model for IV administration of the proteins. The average estimated values (± standard deviation) of σ_{tight} and σ_{leaky} for nineteen mAbs are 0.87 ± 0.20 and 0.57 ± 0.17, respectively, which are within the ranges reported in the literature [36,49]. However, in order to obtain tighter fitting with IV data, σ_{tight} is actually smaller, compared with σ_{leaky}, of three mAbs (Erenumab, Golimumab, and Tralokinumab). A similar "anomaly" is also seen in the literature when mPBPK was used to model the mAbs [49]. Mathematically derived from two reflection coefficients, the concentration ratios of the mAbs in the interstitial fluid vs. plasma are 16% and 54% in tight and leaky tissues, respectively. Other than the three mAbs, the values suggest that tight tissue is almost inaccessible, and albumin is two-fold more permeable to the vasculature in leaky tissue than larger mAbs. These calculated reflection coefficients are in line with the reported size-dependent tissue permeabilities of macromolecules [86].Nonetheless, as further discussed below, mechanistical interpretation of these PK parameters should be taken with caution.

The systemic lymph clearance was found to be more decisive in better fitting the plasma PK profiles of the studied biologics than only with the clearance term by the plasma compartment. The mean (± standard deviation) of the calculated CL_{ly} is 0.062 ± 0.050 L/h for the mAbs, and 0.064 L/h for albumin. CL_{ly} values are larger than the reported plasma clearance (CL_p; 0.018 ± 0.015 L/h) in an mPBPK model with just the CL_p [49]. Given CL_p being assigned zero in this study, the values of lymph and plasma clearance may be only mathematically meaningful. The deficiency likely stems from the overly simplified framework by mPBPK in treating human physiology regarding the transport, disposition, and catabolism of biomolecular drugs. No significant differences in σ_{tight}, σ_{leaky} and CL_{ly} were observed among different IgG isotypes (IgG_1, IgG_2, or IgG_4), light chain types (κ or λ), or sources (human or humanized). Overall, the mPBPK model with drug-specific reflection coefficients and clearance could mathematically reproduce the clinical PK profiles of albumin and therapeutic mAbs following IV administration with reasonable precision (NMSE ranges from 0.09% to 10%; Table 3).

Table 3
Estimated pharmacokinetic parameters for albumin and therapeutic mAbs following IV administration under the assumption that the systemic clearance stems from the systemic lymph compartment. Estimated values are represented as mean ± standard error. σ_{tight} and σ_{leaky} are reflection coefficient in tight tissue and leaky tissue; CL_{ly} is systemic lymphatic clearance; NMSE is normalized mean squared error.

Drug	σ_{tight}	σ_{leaky}	CL_{ly} (L/h)	NMSE
Albumin	1.000 ± 0.028	0.150 ± 0.028	0.064 ± 0.003	0.025
Adalimumab	1.000 ± 0.022	0.479 ± 0.038	0.047 ± 0.006	0.008
Anifrolumab	0.858 ± 0.311	0.727 ± 0.198	0.103 ± 0.031	0.011
Belimumab	1.000 ± 0.086	0.498 ± 0.059	0.037 ± 0.005	0.006
Brodalumab	1.000 ± 0.151	0.314 ± 0.183	0.090 ± 0.018	0.005
Canakinumab	0.948 ± 0.053	0.591 ± 0.038	0.030 ± 0.001	0.001
Daclizumab	0.983 ± 0.194	0.572 ± 0.133	0.055 ± 0.008	0.011
Denosumab	1.000 ± 0.016	0.667 ± 0.021	0.020 ± 0.002	0.008
Dupilumab	1.000 ± 0.001	0.541 ± 0.039	0.042 ± 0.006	0.011
Emicizumab	0.897 ± 0.417	0.527 ± 0.294	0.032 ± 0.008	0.017
Erenumab	0.396 ± 0.664	0.828 ± 0.483	0.039 ± 0.018	0.007
Golimumab	0.394 ± 0.162	0.751 ± 0.097	0.127 ± 0.013	0.001
Guselkumab	0.954 ± 0.440	0.284 ± 0.269	0.053 ± 0.013	0.098
Mepolizumab	1.000 ± 0.013	0.674 ± 0.016	0.043 ± 0.004	0.005
Risankizumab	0.685 ± 0.242	0.674 ± 0.155	0.029 ± 0.006	0.017
Romosozumab	1.000 ± 0.048	0.504 ± 0.039	0.066 ± 0.007	0.004
Sirukumab	0.796 ± 0.214	0.495 ± 0.131	0.070 ± 0.008	0.007
Tildrakizumab	1.000 ± 0.013	0.507 ± 0.049	0.023 ± 0.005	0.014
Tocilizumab	1.000 ± 0.009	0.254 ± 0.036	0.235 ± 0.055	0.009
Tralokinumab	0.616 ± 0.116	0.876 ± 0.077	0.048 ± 0.005	0.002

3.2. Initial lymphatic clearance of albumin

With the drug-specific parameters derived from the clinical data of IV administration in humans and the local absorption kinetics following the SC injection that was simulated by our multiphysics method [31,32], it is possible to derive the clearance for albumin by the initial lymph compartment (CL_{lo}). Once again, our overall PK modeling framework for SC injections of biologics has three essential components (Fig. 1): absorption at the injection site, transit through the initial lymph, and systemic circulation. While the local absorption kinetics and systemic PK parameters can be obtained by the multiphysics simulation and data-fitting of IV clinical data, respectively, CL_{lo} of macromolecules is not readily available in the literature. For albumin, the local clearance could be obtained by fitting the overall simulation and modeling framework against the plasma profile of SC injection, which is available in the literature.

In our multiphysics model of SC absorption, the interplay of tissue mechanics, interstitial fluid flow, and drug mass transport in the SC tissue was computed [31,32]. The absorption kinetics of 1 mg albumin injected into the SC tissue was simulated with inputs of physical attributes of albumin and tissue properties of the human subcutis. Albumin was predicted to be retained at the injection site for two weeks (Fig. 2). The time profile of albumin amount remaining in the SC tissue was then fitted with an exponential function ($m_{albumin} = 1.012\ e^{-0.375\ t}$), used as the input kinetics of SC absorption in the mPBPK model (Eq. 4), with the data-fitted reflection coefficients and systemic clearance from its IV data (Table 3). The simulated local kinetics closely resembles the measured data of the drug concentration in skin (Fig. 2). CL_{lo} of albumin was approximated to be 0.014 L/h, which gives rise to a good match between the observed and the computed SC PK profile (NMSE = 6%), shown in Fig. 2. SC bioavailability of albumin based on the calculated AUC_∞ was estimated to be 82% (while that based on AUC_t was 60%). Note again that both experimental IV and SC plasma profiles of albumin were needed to derive the CL_{lo}. In the reported clinical trial, radio-iodinated albumin was injected intravenously and subcutaneously in the healthy volunteers (N = 5), respectively [54]. The radioactivity of albumin remaining at the injection site and its appearance in the plasma after administration were measured simultaneously using a gamma-spectrometer. Using the radiolabeled protein thus excluded endogenous proteins in the body.

With the computed PBPK parameters using IV and SC PK data, sensitivity analysis was conducted to explore the influence by local absorption kinetics on the systemic distribution of albumin. Based on our early study of the SC multiphysics model, the intrinsic tissue porosity

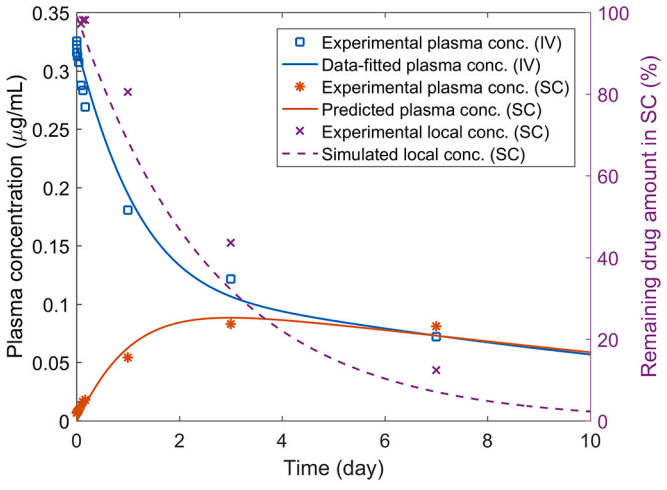

Fig. 2. Simulated and observed PK profiles of IV and SC administration for albumin. Simulated local absorption profile of albumin was generated by multiphysics simulation.

(ϕ_0), lymphatic vessel surface area density (S_{ly}/V), drug partition coefficient (K_p) and lymphatic hydraulic conductivity ($L_{p,\ ly}$) were identified as critical determinants for the absorption rate of albumin in the subcutis [31,32]. Fig. 3 depicts how these tissue properties or drug attributes impact the local absorption kinetics and systemic exposure following SC administration. A smaller ϕ_0, or a larger S_{ly}/V, K_p, or $L_{p,\ ly}$ can dramatically accelerate the absorption from the injection site, leading to a higher C_{max} and a smaller T_{max}, while the bioavailability remains to be relatively similar. Additionally, modeling of the physiological parameters of initial lymphatics shows that the volume of initial lymphatics (V_{lo}), reported to vary among different injection sites (arm, thigh and abdomen) [25], has minimal impact on the SC PK. Conversely, a higher clearance (CL_{lo}) or a lower flow rate (L_{lth}) of the initial lymphatic compartment reduces the C_{max} and bioavailability but with no effect on T_{max}. Increasing CL_{lo} from 0.5- to 1.5-fold of the derive value (0.014 L/h) reduces C_{max} or bioavailability from 110% to 91%; decreasing L_{lth} from 1.7- to 0.7-fold of the literature value (0.060 L/h) reduces C_{max} or bioavailability from 108% to 91%.

3.3. Initial lymphatic clearance and local absorption of mAbs

Unfortunately, for the therapeutic mAbs whose systemic disposition parameters could be estimated from their respective IV profiles (Table 3), there is no experimental data reported in the literature of local drug concentrations at the injection site in humans. Nor is there reliable data of their respective physicochemical properties such as diffusivity and membrane permeability to conduct reliable simulation of local absorption kinetics. Given these challenges, we conducted two sets of simulation experiments under two assumptions to explore the possible extents of the pre-systemic clearance and local absorption kinetics of

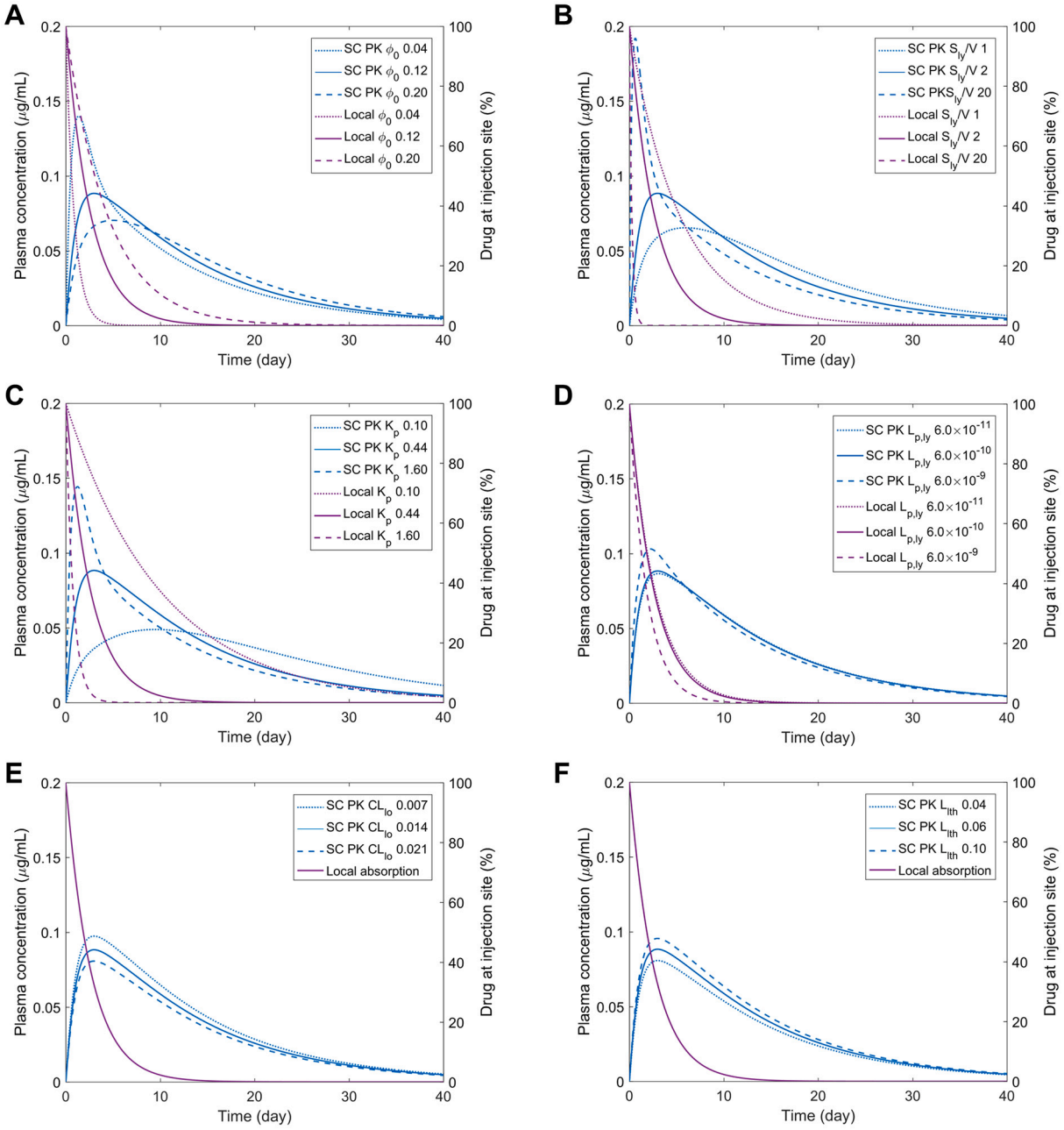

Fig. 3. The time profiles of drug remaining at the injection site and plasma concentration-time profile of 1 mg albumin following SC administration, given the respective values of intrinsic tissue porosity (ϕ_0), lymphatic vessel surface area density (S_{ly}/V; unit: cm^{-1}), drug partition coefficient (K_p) and lymphatic hydraulic conductivity ($L_{p,\ ly}$; unit: cm/(Pa•s)), initial lymphatic clearance (CL_{lo}; unit: L/h), and flow rate of thoracic duct (L_{lth}; unit: L/h).

these mAbs.

First, we assumed that the mAbs share the same local absorption kinetics as IgG. This is unlikely, but it allows us to evaluate the clearance in the initial lymphatic compartment. In our earlier study, the local simulation of subcutaneously injected IgG was conducted with its physicochemical properties obtained from the literature [31,32]. The local kinetics seemed to follow the experimental observation in which radio-labelled polyclonal IgG was subcutaneously injected to humans and measured, although measurements within the first six hours were reported [87]. The simulated time-course of IgG amount remaining in the subcutis after injection of 50 mg was then fitted by an exponential equation ($m_{IgG} = 50.400\ e^{-0.211\ t}$) and used in integrating with the mPBPK model. Table 4 lists the CL_{lo} values of mAbs that were derived by using the local absorption kinetics of IgG and systemic PK parameters in generating plasma profiles and comparing against respectively observed SC PK data. The CL_{lo} values of mAbs are averaged as 0.046 ± 0.037 L/h, ranging from 0.003 (Anifrolumab) to 0.134 L/h (Tocilizumab). The average is close to the systemic clearance (CL_{ly}) of mAbs with the average of 0.062 ± 0.050 L/h ($P = 0.09$) and ranging from 0.020 (Denosumab) to 0.235 L/h (Tocilizumab). Individual comparisons between CL_{lo} and CL_{ly} of mAbs is shown in Tables 3 and 4, indicating a positive correlation (Pearson coefficient, $r = 0.59$). CL_{lo} is also highly correlated with the SC bioavailability reported in literature (Table 4; $r = -0.88$). CL_{lo} represents the presystemic catabolism of biologics in the draining lymph from the injection site prior to entering the systemic circulation, which has been reported to be negatively related with the bioavailability of biologics [21,88]. This is also consistent with earlier findings of a negative relationship between the SC bioavailability and IV clearance of mAb products in humans [89] and minipigs [90]. This correlation implies similar catabolic mechanisms and kinetic processes between the systemic and presystemic clearance. Interestingly, CL_{lo} shows a negative correlation with the inaccessible capillary membrane fraction in leaky tissue (σ_{leaky}, Table 3; $r = -0.58$). This suggests that leaky tissue (liver, kidney, and heart) with less restriction to drug transport contributes more to protein degradation, which may occur mostly in the interstitial fluid or draining lymph. This is supported by a reported study in which antibodies with more extensive tissue disposition is associated with higher systemic clearance [91].

Attempts to correlate CL_{lo} with formulation-relevant or physicochemical properties of mAbs were made, with the Pearson coefficients (r) listed in Table 5. CL_{pl} was found to have a relatively meaningful correlation with the predicted aggregation tendency of the beta-sheet in heavy chain of mAbs ($r = -0.53$). Among the measured biophysical properties, the melting temperature (Tm) of the antigen-binding fragment (Fab) of sixteen mAbs seems to bear a connection with CL_{lo} ($r = 0.63$). A recent study reports that higher Tm is associated with larger degree of degradation mAbs [92]. This might suggest that the presystemic clearance – as well as the systemic clearance – of a mAb is associated with the structural stability of antibodies.

Second, by assuming that the local clearance is the same as the respective systemic clearance of each mAb, we could derive the local absorption kinetics and compare with that of IgG. More specifically, the coefficient a in the exponential function of respective absorption kinetics was calculated and listed in Table 6. The calculated coefficient has an average value of −0.296 ± 0.084 d^{-1}, ranging from −0.482 d^{-1} (Tocilizumab) to −0.166 d^{-1} (Emicizumab). A less negative a value (a larger a) indicates a slower drug disappearance rate from the SC injection site. The average estimated a of nineteen mAbs is significantly different from that of IgG (−0.211 d^{-1}), which was derived from the multiphysics simulation. Fig. 4 illustrates the derived profiles of local absorption kinetics of the mAbs, showing possible variations in

Table 5
Pearson correlation coefficients of CL_{lo} and a against various formulation and biophysical properties. CL_{lo} is initial lymphatic clearance; a is absorption rate coefficient.

Properties	CL_{lo}	a
Molecular weight	0.175	−0.234
Formulation pH	−0.215	0.110
Isoelectric point (pI)	0.144	0.060
Difference between pI and pH 7.4	0.373	0.123
Charge at pH 7.4	0.240	−0.005
Charge at formulation pH	0.333	−0.072
Scaled solubility	0.253	0.224
Aggregation tendency of beta-sheet in heavy chain	−0.534	0.226
Aggregation tendency of beta-sheet in light chain	−0.264	0.252
Patches of surface hydrophobicity metric in CDR	−0.103	0.220
Patches of positive charge metric in CDR	−0.079	0.562
Patches of negative charge metric in CDR	−0.008	−0.266
Expression titer in HEK cells	0.314	−0.243
Melting temperature of the Fab (Tm)	0.633	−0.643
Salt-gradient affinity-capture self-interaction nanoparticle spectroscopy (SGAC-SINS AS100) assay	0.322	−0.136
Retention time in hydrophobic interaction chromatography (HIC)	−0.262	0.236
Delta response of clone self-interaction by biolayer interferometry (CSI-BLI)	−0.151	0.410
Baculovirus particle (BVP) ELISA assay	−0.090	0.265

Table 4
Estimated initial lymphatic clearance (CL_{lo}) of 50 mg mAbs. Bioavailability was obtained from analyzing the PK data from references listed in Table 2. Estimated values are represented as mean ± standard error. NMSE is normalized mean squared error.

Drug	CL_{lo} (L/h)	NMSE	Bioavailability
Adalimumab	0.071 ± 0.010	0.138	0.52
Anifrolumab	0.003 ± 0.003	0.046	0.90
Belimumab	0.008 ± 0.002	0.034	0.81
Brodalumab	0.122 ± 0.016	0.189	0.24
Canakinumab	0.017 ± 0.002	0.035	0.77
Daclizumab	0.038 ± 0.005	0.070	0.85
Denosumab	0.034 ± 0.001	0.015	0.59
Dupilumab	0.067 ± 0.016	0.282	0.52
Emicizumab	0.022 ± 0.022	0.048	0.80
Erenumab	0.047 ± 0.005	0.069	0.51
Golimumab	0.046 ± 0.003	0.037	0.55
Guselkumab	0.075 ± 0.028	0.015	0.48
Mepolizumab	0.031 ± 0.002	0.031	0.71
Risankizumab	0.039 ± 0.002	0.007	0.70
Romosozumab	0.070 ± 0.010	0.207	0.59
Sirukumab	0.008 ± 0.003	0.068	0.75
Tildrakizumab	0.005 ± 0.003	0.080	0.74
Tocilizumab	0.134 ± 0.035	0.636	0.40
Tralokinumab	0.030 ± 0.003	0.032	0.62

Table 6
Estimated exponential coefficient a in local absorption kinetics of 50-mg mAbs in SC tissue. Estimated values are represented as mean ± standard error. a is absorption rate coefficient; NMSE is normalized mean squared error.

Drug	a (d^{-1})	NMSE
Adalimumab	−0.352 ± 0.564	0.056
Anifrolumab	−0.294 ± 0.024	0.019
Belimumab	−0.274 ± 0.016	0.013
Brodalumab	−0.387 ± 0.058	0.056
Canakinumab	−0.272 ± 0.016	0.012
Daclizumab	−0.306 ± 0.045	0.045
Denosumab	−0.195 ± 0.008	0.013
Dupilumab	−0.355 ± 0.121	0.177
Emicizumab	−0.166 ± 0.015	0.031
Erenumab	−0.208 ± 0.029	0.069
Golimumab	−0.290 ± 0.020	0.014
Guselkumab	−0.218 ± 0.015	0.015
Mepolizumab	−0.261 ± 0.015	0.018
Risankizumab	−0.213 ± 0.013	0.007
Romosozumab	−0.454 ± 0.048	0.033
Sirukumab	−0.319 ± 0.036	0.033
Tildrakizumab	−0.325 ± 0.026	0.024
Tocilizumab	−0.482 ± 0.190	0.336
Tralokinumab	−0.256 ± 0.022	0.022

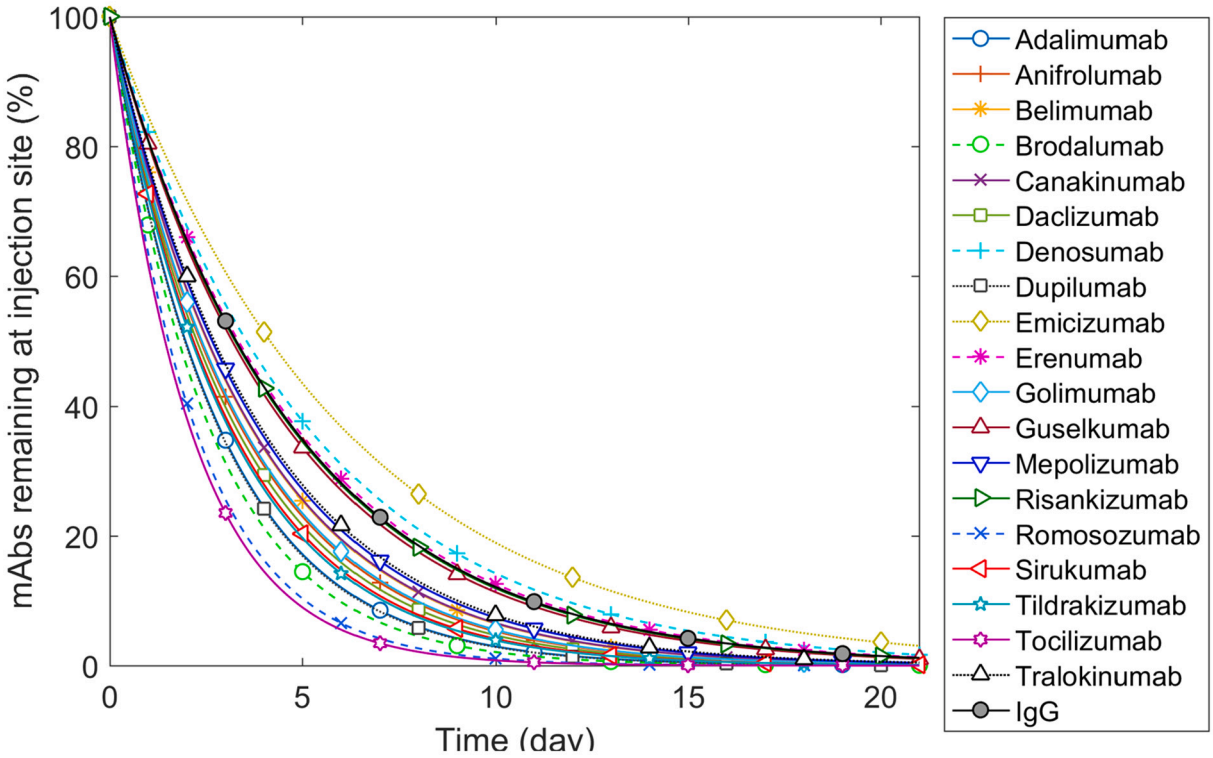

Fig. 4. Overlay of derived local absorption profiles of mAbs at 50 mg dose. IgG_1-, IgG_2- and IgG_4-isotype mAbs are shown as solid, dashed, and dotted lines, respectively.

absorption rate among the mAbs with no apparent distinction among different isotypes. Based on our previous report [31,32], the absorption rate at the injection site is mostly sensitive to the partition coefficient of a protein across the lymphatic membrane (Fig. 3C), which likely varies among the mAb products.

The computed absorption coefficient a shows a relatively strong correlation with the derived systemic clearance values (CL_{ly}, Table 3; $r = -0.63$). The trend suggests that faster local absorption (a smaller a) is associated with quicker systemic clearance. This interesting implication is corroborated by a reported finding of a positive relationship between the local absorption rate of SC delivery and IV clearance in a two-compartment PK model [89]. Additionally, to some degrees, the rate coefficient seems to be associated with the bioavailability ($r = 0.39$) and tissue reflection coefficients (σ_{leaky}, $r = 0.51$; σ_{tight}, $r = 0.37$). These possible connections imply that restricted tissue distribution and reduced local absorption rates may share similar structural causes.

Among the physiochemical properties of the nineteen mAbs investigated, the positive charge value in the CDRs is positively associated with the coefficient a ($r = 0.56$). This is consistent with the reported finding that higher positive charge in the solvent-accessible area of a mAb can significantly deter the SC absorption, likely due to stronger electrostatic interactions with the negatively charged interstitial constituents and longer retention in subcutis [91]. Moreover, Tm seems to be negatively correlated with the absorption coefficient among sixteen mAbs ($r = -0.64$), underlying some connection between the local absorption kinetics and structural stability of mAbs.

Obviously, for an mAb that is subcutaneously injected, its initial lymphatic clearance may not be the same as the systemic value and its absorption kinetics at the injection site should be distinct from that of IgG. While the two assumptions used in the computational exercises may represent two simplified extremes between which the actual kinetics resides, the correlation results discussed above can still shed some light on the presystemic catabolism and local absorption kinetics. The presystemic clearance may be related with the aggregation propensity of mAbs, while the local absorption rate seems to be linked with the positive charge exposed in the antigen-binding domain.

While coupling the physics-based simulation of injection-site absorption with the whole-body PK modeling (mPBPK) demonstrates the feasibility to predict the in vivo exposure of locally administered protein solutions, it is worthy to note that our multiscale framework reveals several general knowledge gaps impeding its applications. In addition to the initial lymphatic clearance remaining unknown in our PK model a priori, limited experimental evidence is available in the literature regarding possible catabolism and/or self-aggregation kinetics of protein molecules in subcutis, forcing the omission of such events in our local simulation method [31,32]. Possibilities of the local absorption by blood vessels cannot be ruled out, especially for smaller proteins. Moreover, it is speculated that injection of a high-concentration protein solution may induce structure misfolding and self-association, which is explored by our previous simulation of syringe injection [93]. Lastly, the mPBPK model used in this study overly simplifies the treatment of human physiology regarding the transportation, disposition, and catabolism of injected biomolecules, making any comparison between the plasma and lymph clearance perhaps only mathematically meaningful. Lack of understanding in these areas needs broader and in-depth investigations with animal models, clinical studies, and molecular characterization and modeling.

4. Summary

In this study, a multiscale simulation and modeling framework was developed to compute the systemic exposure and bioavailability of subcutaneously administrated biotherapeutics. The method integrates the multiphysics simulation of drug absorption kinetics at the injection site with the whole-body PK modeling of systemic disposition. In addition, the presystemic clearance by initial lymph flow is modeled to bridge the local absorption and systemic circulation. While the simulation of local transport and absorption of a protein is conducted via first principles, the PK modeling requires empirical parameters obtained by fitting against clinical data. With a lack of knowledge regarding the

initial clearance of biopharmaceuticals, this study demonstrated the application of the multiscale PK framework for assessing the presystemic PK and bioavailability of selected biomolecules. Correlation of the local and presystemic kinetics with formulation and molecular properties was attempted, shedding light on tissue transport mechanisms of large molecules.

This study also highlighted the need to experimentally determine and understand how a protein molecule undergoes various steps traversing from the injection site to systemic circulation. The need to evaluate the structural change, both physical and chemical, in the subcutis and lymph cannot be overstressed. The knowledge gained from such studies will further improve the multiscale simulation and modeling framework to eventually predict the bioavailability of a given protein or antibody product locally administered, leading to in silico evaluation of the impact by critical quality attributes of the formulation and/or change of the administration route (e.g., using microneedle) on the systemic exposure.

Acknowledgement

The authors acknowledge the support by Purdue Research Foundation and the Digital Human project by the Weldon School of Biomedical Engineering at Purdue University.

References

[1] K.C. Anderson, O. Landgren, R.C. Arend, J. Chou, I.A. Jacobs, Humanistic and economic impact of subcutaneous versus intravenous Administration of Oncology Biologics, Future Oncol. 15 (2019) 3267–3281.
[2] A.L. Grilo, A. Mantalaris, The increasingly human and profitable monoclonal antibody market, Trends Biotechnol. 37 (2019) 9–16.
[3] D.M. Ecker, S.D. Jones, H.L. Levine, The therapeutic monoclonal antibody market, mAbs 7 (2015) 9–14.
[4] M. Viola, J. Sequeira, R. Seiça, F. Veiga, J. Serra, A.C. Santos, A.J. Ribeiro, Subcutaneous delivery of monoclonal antibodies: how do we get there? J. Control. Release 286 (2018) 301–314.
[5] S.S. Usmani, G. Bedi, J.S. Samuel, S. Singh, S. Kalra, P. Kumar, A.A. Ahuja, M. Sharma, A. Gautam, G.P.S. Raghava, Thpdb: database of Fda-approved peptide and protein therapeutics, PLoS One 12 (2017), e0181748.
[6] B. Bittner, W. Richter, J. Schmidt, Subcutaneous Administration of Biotherapeutics: an overview of current challenges and opportunities, BioDrugs 32 (2018) 425–440.
[7] A. Datta-Mannan, Mechanisms influencing the pharmacokinetics and disposition of monoclonal antibodies and peptides, Drug Metab. Dispos. 47 (2019) 1100.
[8] T.A. McDonald, M.L. Zepeda, M.J. Tomlinson, W.H. Bee, I.A. Ivens, Subcutaneous Administration of Biotherapeutics: current experience in animal models, Curr. Opin. Mol. Ther. 12 (2010) 461–470.
[9] L.T. Baxter, R.K. Jain, Transport of fluid and macromolecules in tumors. I. Role of interstitial pressure and convection, Microvasc. Res. 37 (1989) 77–104.
[10] J.R. Levick, C.C. Michel, Microvascular fluid exchange and the revised Starling principle, Cardiovasc. Res. 87 (2010) 198–210.
[11] A. Supersaxo, W.R. Hein, H. Steffen, Effect of molecular weight on the lymphatic absorption of water-soluble compounds following subcutaneous administration, Pharm. Res. 7 (1990) 167–169.
[12] M.A. Swartz, The physiology of the lymphatic system, Adv. Drug Deliv. Rev. 50 (2001) 3–20.
[13] D.N. McLennan, C.J.H. Porter, G.A. Edwards, S.W. Martin, A.C. Heatherington, S. A. Charman, Lymphatic absorption is the primary contributor to the systemic availability of Epoetin Alfa following subcutaneous administration to sheep, J. Pharmacol. Exp. Ther. 313 (2005) 345–351.
[14] D.N. McLennan, C.J. Porter, G.A. Edwards, M. Brumm, S.W. Martin, S.A. Charman, Pharmacokinetic model to describe the lymphatic absorption of R-Methu-Leptin after subcutaneous injection to sheep, Pharm. Res. 20 (2003) 1156–1162.
[15] A.M. Dahlberg, L.M. Kaminskas, A. Smith, J.A. Nicolazzo, C.J. Porter, J.B. Bulitta, M.P. McIntosh, The lymphatic system plays a major role in the intravenous and subcutaneous pharmacokinetics of Trastuzumab in rats, Mol. Pharm. 11 (2014) 496–504.
[16] I.K. Styles, O.M. Feeney, T.H. Nguyen, D.H.S. Brundel, D.W. Kang, R. Clift, M. P. McIntosh, C.J.H. Porter, Removal of interstitial Hyaluronan with recombinant human Hyaluronidase improves the systemic and lymphatic uptake of Cetuximab in rats, J. Control. Release 315 (2019) 85–96.
[17] H.M. Kinnunen, R.J. Mrsny, Improving the outcomes of biopharmaceutical delivery via the subcutaneous route by understanding the chemical, physical and physiological properties of the subcutaneous injection site, J. Control. Release 182 (2014) 22–32.
[18] W.F. Richter, S.G. Bhansali, M.E. Morris, Mechanistic determinants of biotherapeutics absorption following Sc administration, AAPS J. 14 (2012) 559–570.
[19] J.A.D. Sequeira, A.C. Santos, J. Serra, C. Estevens, R. Seiça, F. Veiga, A.J. Ribeiro, Subcutaneous delivery of biotherapeutics: challenges at the injection site, Expert. Opin. Drug. Deliv. 16 (2019) 143–151.
[20] M.R. Turner, S.V. Balu-Iyer, Challenges and opportunities for the subcutaneous delivery of therapeutic proteins, J. Pharm. Sci. 107 (2018) 1247–1260.
[21] W.F. Richter, B. Jacobsen, Subcutaneous absorption of biotherapeutics: Knowns and unknowns, Drug Metab. Dispos. 42 (2014) 1881–1889.
[22] D.S. Collins, M. Sánchez-Félix, A.V. Badkar, R. Mrsny, Accelerating the development of novel technologies and tools for the subcutaneous delivery of biotherapeutics, J. Control. Release 321 (2020) 475–482.
[23] M. Dostalek, I. Gardner, B.M. Gurbaxani, R.H. Rose, M. Chetty, Pharmacokinetics, pharmacodynamics and physiologically-based pharmacokinetic Modelling of monoclonal antibodies, Clin. Pharmacokinet. 52 (2013) 83–124.
[24] L. Kagan, D.E. Mager, Mechanisms of subcutaneous absorption of rituximab in rats, Drug Metab. Dispos. 41 (2013) 248–255.
[25] N. Varkhede, L. Forrest, Understanding the monoclonal antibody disposition after subcutaneous administration using a minimal physiologically based pharmacokinetic model, J. Pharm. Pharm. Sci. 21 (2018) 130s–148s.
[26] C.J. Porter, S.A. Charman, Lymphatic transport of proteins after subcutaneous administration, J. Pharm. Sci. 89 (2000) 297–310.
[27] Y.M. Wang, J. Wang, Y.Y. Hon, L. Zhou, L. Fang, H.Y. Ahn, Evaluating and reporting the immunogenicity impacts for biological products–a clinical pharmacology perspective, AAPS J. 18 (2016) 395–403.
[28] J.Q. Dong, D.H. Salinger, C.J. Endres, J.P. Gibbs, C.-P. Hsu, B.J. Stouch, E. Hurh, M. Gibbs, Quantitative prediction of human pharmacokinetics for monoclonal antibodies, Clin. Pharmacokinet. 50 (2011) 131–142.
[29] M. Sánchez-Félix, M. Burke, H.H. Chen, C. Patterson, S. Mittal, Predicting bioavailability of monoclonal antibodies after subcutaneous administration: open innovation challenge, Adv. Drug Deliv. Rev. 167 (2020) 66–77.
[30] D.S. Collins, L.C. Kourtis, N.R. Thyagarajapuram, R. Sirkar, S. Kapur, M. W. Harrison, D.J. Bryan, G.B. Jones, J.M. Wright, Optimizing the bioavailability of subcutaneously administered biotherapeutics through Mechanochemical drivers, Pharm. Res. 34 (2017) 2000–2011.
[31] F. Zheng, P. Hou, C.D. Corpstein, L. Xing, T. Li, Multiphysics modeling and simulation of subcutaneous injection and absorption of biotherapeutics: model development, Pharm. Res. 38 (2021) 607–624.
[32] P. Hou, F. Zheng, C.D. Corpstein, L. Xing, T. Li, Multiphysics modeling and simulation of subcutaneous injection and absorption of biotherapeutics: sensitivity analysis, Pharm. Res. 38 (2021) 1011–1030.
[33] E. Detournay, A.H.D. Cheng, 5 - fundamentals of Poroelasticity, in: C. Fairhurst (Ed.), Analysis and Design Methods, Pergamon, Oxford, 1993, pp. 113–171.
[34] H. Darcy, *Les Fontaines Publiques De La Ville De Dijon: Exposition Et Application Des Principes À Suivre Et Des Formules À Employer Dans Les Questions De Distribution D'eau : Ouvrage Terminé Par Un Appendice Relatif Aux Fournitures D'eau De Plusieurs Villes, Au Filtrage Des Eaux Et À La Fabrication Des Tuyaux De Fonte, De Plomb, De Tôle Et De Bitume*. ed.; V. Dalmont, 1856.
[35] J. Scallan, V.H. Huxley, R.J. Korthuis, Integrated systems physiology: from molecule to function to disease, in: Capillary Fluid Exchange: Regulation, Functions, and Pathology, Morgan & Claypool Life Sciences, San Rafael (CA), 2010.
[36] Y. Cao, J.P. Balthasar, W.J. Jusko, Second-generation minimal physiologically-based pharmacokinetic model for monoclonal antibodies, J. Pharmacokinet. Pharmacodyn. 40 (2013) 597–607.
[37] J.O. Jørgensen, A. Flyvbjerg, T. Lauritzen, H. Orskov, J.S. Christiansen, Subcutaneous degradation of biosynthetic human growth hormone in growth hormone deficient patients, Acta Endocrinol. 118 (1988) 154–158.
[38] M. Berger, P.A. Halban, L. Girardier, J. Seydoux, R.E. Offord, A.E. Renold, Absorption kinetics of subcutaneously injected insulin, Diabetologia 17 (1979) 97–99.
[39] K. Okumura, F. Komada, R. Hori, Fate of porcine and human insulin at the subcutaneous injection site. I. Degradation and absorption of Insulins in the rat, Aust. J. Pharm. 8 (1985) 25–32.
[40] W. Wang, N. Chen, X. Shen, P. Cunningham, S. Fauty, K. Michel, B. Wang, X. Hong, C. Adreani, C.N. Nunes, C.V. Johnson, K.-C. Yin, M. Groff, Y. Zou, L. Liu, L. Hamuro, T. Prueksaritanont, Lymphatic transport and catabolism of therapeutic proteins after subcutaneous administration to rats and dogs, Drug Metab. Dispos. 40 (2012) 952–962.
[41] J.A. Parsons, B. Rafferty, R.W. Stevenson, J.M. Zanelli, Evidence that protease inhibitors reduce the degradation of parathyroid hormone and calcitonin injected subcutaneously, Br. J. Pharmacol. 66 (1979) 25–32.
[42] H. Sarin, Physiologic upper limits of pore size of different blood capillary types and another perspective on the dual pore theory of microvascular permeability, J. Angiogenes. Res. 2 (2010) 14.
[43] T. Stylianopoulos, L.L. Munn, R.K. Jain, Reengineering the physical microenvironment of tumors to improve drug delivery and efficacy: from mathematical modeling to bench to bedside, Trends Cancer 4 (2018) 292–319.
[44] D.K. Shah, A.M. Betts, Towards a platform Pbpk model to characterize the plasma and tissue disposition of monoclonal antibodies in preclinical species and human, J. Pharmacokinet. Pharmacodyn. 39 (2012) 67–86.
[45] R.W. Pain, Body fluid compartments, Anaesth. Intensive Care 5 (1977) 284–294.
[46] C. Giragossian, C. Vage, J. Li, K. Pelletier, N. Piché-Nicholas, M. Rajadhyaksha, J. Liras, A. Logan, R.A. Calle, Y. Weng, Mechanistic investigation of the preclinical pharmacokinetics and interspecies scaling of Pf-05231023, a fibroblast growth factor 21-antibody protein conjugate, Drug Metab. Dispos. 43 (2015) 803–811.
[47] A.E. Dumont, J.H. Mulholland, Flow rate and composition of thoracic-duct lymph in patients with cirrhosis, N. Engl. J. Med. 263 (1960) 471–474.

[48] O. Stücker, C. Pons-Himbert, E. Laemmel, Towards a better understanding of lymph circulation, Phlebolymphology 15 (2008) 31–36.
[49] Y. Cao, W.J. Jusko, Survey of monoclonal antibody disposition in man utilizing a minimal physiologically-based pharmacokinetic model, J. Pharmacokinet. Pharmacodyn. 41 (2014) 571–580.
[50] A. Garg, J.P. Balthasar, Physiologically-based pharmacokinetic (Pbpk) model to predict igg tissue kinetics in wild-type and Fcrn-knockout mice, J. Pharmacokinet. Pharmacodyn. 34 (2007) 687–709.
[51] H. Wiig, O. Tenstad, Interstitial exclusion of positively and negatively charged igg in rat skin and muscle, Am. J. Physiol. Heart Circ. Physiol. 280 (2001) H1505–H1512.
[52] H. Wiig, G.A. Kaysen, H.A. Al-Bander, M. De Carlo, L. Sibley, E.M. Renkin, Interstitial exclusion of igg in rat tissues estimated by continuous infusion, Am. J. Phys. 266 (1994) H212–H219.
[53] H. Wiig, M. DeCarlo, L. Sibley, E.M. Renkin, Interstitial exclusion of albumin in rat tissues measured by a continuous infusion method, Am. J. Phys. 263 (1992) H1222–H1233.
[54] M.T. Hays, R.A. McGuire, Distribution of subcutaneous Thyroxine, Triiodothyronine, and albumin in man: comparison with intravenous administration using a kinetic model, J. Clin. Endocrinol. Metab. 51 (1980) 1112–1117.
[55] Center for Drug Evaluation and Research and Center for Biologics Evaluation and Research, F, Adalimumab Clinical Pharmacology and Biopharmaceutics Reviews, 2002.
[56] R. Tummala, T. Rouse, A. Berglind, L. Santiago, Safety, tolerability and pharmacokinetics of subcutaneous and intravenous anifrolumab in healthy volunteers, Lupus. Sci. Med. 5 (2018), e000252.
[57] W.W. Cai, M. Fiscella, C. Chen, Z.J. Zhong, W.W. Freimuth, D.C. Subich, Bioavailability, pharmacokinetics, and safety of Belimumab administered subcutaneously in healthy subjects, Clin. Pharmacol. Drug Dev. 2 (2013) 349–357.
[58] D.H. Salinger, C.J. Endres, D.A. Martin, M.A. Gibbs, A semi-mechanistic model to characterize the pharmacokinetics and pharmacodynamics of Brodalumab in healthy volunteers and subjects with psoriasis in a first-in-human single ascending dose study, Clin. Pharmacol. Drug Dev. 3 (2014) 276–283.
[59] A. Chakraborty, S. Tannenbaum, C. Rordorf, P.J. Lowe, D. Floch, H. Gram, S. Roy, Pharmacokinetic and Pharmacodynamic properties of Canakinumab, a human anti-interleukin-1β monoclonal antibody, Clin. Pharmacokinet. 51 (2012) e1–18.
[60] L. Diao, Y. Hang, A.A. Othman, I. Nestorov, J.Q. Tran, Population pharmacokinetics of Daclizumab high-yield process in healthy volunteers and subjects with multiple sclerosis: analysis of phase I-iii clinical trials, Clin. Pharmacokinet. 55 (2016) 943–955.
[61] L. Sutjandra, R.D. Rodriguez, S. Doshi, M. Ma, M.C. Peterson, G.R. Jang, A. T. Chow, J.J. Pérez-Ruixo, Population pharmacokinetic meta-analysis of Denosumab in healthy subjects and postmenopausal women with osteopenia or osteoporosis, Clin. Pharmacokinet. 50 (2011) 793–807.
[62] Z. Li, A. Radin, M. Li, J.D. Hamilton, M. Kajiwara, J.D. Davis, Y. Takahashi, S. Hasegawa, J.E. Ming, A.T. DiCioccio, Y. Li, P. Kovalenko, Q. Lu, C. Ortemann-Renon, M. Ardeleanu, B.N. Swanson, Pharmacokinetics, pharmacodynamics, safety, and tolerability of Dupilumab in healthy adult subjects, Clin. Pharmacol. Drug Dev. 9 (2020) 742–755.
[63] N. Kotani, K. Yoneyama, N. Kawakami, T. Shimuta, H. Fukase, T. Kawanishi, Relative and absolute bioavailability study of Emicizumab to bridge drug products and subcutaneous injection sites in healthy volunteers, Clin. Pharmacol. Drug Dev. 8 (2019) 702–712.
[64] J. de Hoon, A. Van Hecken, C. Vandermeulen, L. Yan, B. Smith, J.S. Chen, E. Bautista, L. Hamilton, J. Waksman, T. Vu, G. Vargas, Phase I, randomized, double-blind, placebo-controlled, single-dose, and multiple-dose studies of Erenumab in healthy subjects and patients with migraine, Clin. Pharmacol. Ther. 103 (2018) 815–825.
[65] Z. Xu, Q. Wang, Y. Zhuang, B. Frederick, H. Yan, E. Bouman-Thio, J.C. Marini, M. Keen, D. Snead, H.M. Davis, H. Zhou, Subcutaneous bioavailability of Golimumab at 3 different injection sites in healthy subjects, J. Clin. Pharmacol. 50 (2010) 276–284.
[66] Y. Zhuang, C. Calderon, S.J. Marciniak Jr., E. Bouman-Thio, P. Szapary, T.Y. Yang, A. Schantz, H.M. Davis, H. Zhou, Z. Xu, First-in-human study to assess Guselkumab (anti-Il-23 Mab) pharmacokinetics/safety in healthy subjects and patients with moderate-to-severe psoriasis, Eur. J. Clin. Pharmacol. 72 (2016) 1303–1310.
[67] H. Ortega, S. Yancey, S. Cozens, Pharmacokinetics and absolute bioavailability of Mepolizumab following Administration at Subcutaneous and Intramuscular Sites, Clin. Pharmacol. Drug Dev. 3 (2014) 57–62.
[68] S. Shabbir, I.J. Pouliquen, J.H. Bentley, E.S. Bradford, M. Albayaty, the pharmacokinetics and relative bioavailability of Mepolizumab 100 mg liquid formulation administered subcutaneously to healthy participants: a randomized trial, Clin. Pharmacol. Drug Dev. 9 (2020) 375–385.
[69] N. Tsukamoto, N. Takahashi, H. Itoh, I. Pouliquen, Pharmacokinetics and pharmacodynamics of Mepolizumab, an anti-interleukin 5 monoclonal antibody, in healthy Japanese male subjects, Clin. Pharmacol. Drug Dev. 5 (2016) 102–108.
[70] A. Khatri, D. Eckert, R. Oberoi, A. Suleiman, Y. Pang, L. Cheng, A.A. Othman, Pharmacokinetics of Risankizumab in Asian healthy subjects and patients with moderate to severe plaque psoriasis, generalized Pustular psoriasis, and Erythrodermic psoriasis, J. Clin. Pharmacol. 59 (2019) 1656–1668.
[71] D. Padhi, G. Jang, B. Stouch, L. Fang, E. Posvar, Single-dose, placebo-controlled, randomized study of Amg 785, a Sclerostin monoclonal antibody, J. Bone Miner. Res. 26 (2011) 19–26.
[72] Z. Xu, E. Bouman-Thio, C. Comisar, B. Frederick, B. Van Hartingsveldt, J.C. Marini, H.M. Davis, H. Zhou, Pharmacokinetics, pharmacodynamics and safety of a human anti-Il-6 monoclonal antibody (Sirukumab) in healthy subjects in a first-in-human study, Br. J. Clin. Pharmacol. 72 (2011) 270–281.
[73] Y. Zhuang, Z. Xu, D.E. de Vries, Q. Wang, A. Shishido, C. Comisar, J.A. Ford, M. Keen, M. Achira, Y. Tsukamoto, K.J. Petty, H.M. Davis, H. Zhou, Pharmacokinetics and safety of Sirukumab following a single subcutaneous administration to healthy Japanese and Caucasian subjects, Int. J. Clin. Pharmacol. Ther. 51 (2013) 187–199.
[74] S. Khalilieh, P. Hodsman, C. Xu, A. Tzontcheva, S. Glasgow, D. Montgomery, Pharmacokinetics of Tildrakizumab (Mk-3222), an anti-Il-23 monoclonal antibody, after intravenous or subcutaneous Administration in Healthy Subjects, Basic Clin. Pharmacol. Toxicol. 123 (2018) 294–300.
[75] X. Zhang, A. Georgy, L. Rowell, Pharmacokinetics and pharmacodynamics of Tocilizumab, a humanized anti-Interleukin-6 receptor monoclonal antibody, following single-dose administration by subcutaneous and intravenous routes to healthy subjects, Int. J. Clin. Pharmacol. Ther. 51 (2013) 443–455.
[76] C.K. Oh, R. Faggioni, F. Jin, L.K. Roskos, B. Wang, C. Birrell, R. Wilson, N. A. Molfino, An open-label, single-dose bioavailability study of the pharmacokinetics of Cat-354 after subcutaneous and intravenous Administration in Healthy Males, Br. J. Clin. Pharmacol. 69 (2010) 645–655.
[77] Tabs - Therapeutic Antibody Database. https://tabs.craic.com/, 2020.
[78] E. Gasteiger, C. Hoogland, A. Gattiker, S. Duvaud, M.R. Wilkins, R.D. Appel, A. Bairoch, Protein identification and analysis tools on the expasy server, in: J. M. Walker (Ed.), The Proteomics Protocols Handbook, Humana Press, Totowa, NJ, 2005, pp. 571–607.
[79] Protein Calculator V3.4. http://protcalc.sourceforge.net/.
[80] M. Hebditch, M.A. Carballo-Amador, S. Charonis, R. Curtis, J. Warwicker, Protein–sol: a web tool for predicting protein solubility from sequence, Bioinformatics 33 (2017) 3098–3100.
[81] O. Conchillo-Solé, N.S. de Groot, F.X. Avilés, J. Vendrell, X. Daura, S. Ventura, Aggrescan: a server for the prediction and evaluation of "hot spots" of aggregation in polypeptides, BMC Bioinformatics 8 (2007) 65.
[82] A.M. Fernandez-Escamilla, F. Rousseau, J. Schymkowitz, L. Serrano, Prediction of sequence-dependent and mutational effects on the aggregation of peptides and proteins, Nat. Biotechnol. 22 (2004) 1302–1306.
[83] M.I.J. Raybould, C. Marks, K. Krawczyk, B. Taddese, J. Nowak, A.P. Lewis, A. Bujotzek, J. Shi, C.M. Deane, Five computational developability guidelines for therapeutic antibody profiling, P Natl Acad Sci 116 (2019) 4025.
[84] T. Jain, T. Sun, S. Durand, A. Hall, N.R. Houston, J.H. Nett, B. Sharkey, B. Bobrowicz, I. Caffry, Y. Yu, Y. Cao, H. Lynaugh, M. Brown, H. Baruah, L.T. Gray, E.M. Krauland, Y. Xu, M. Vásquez, K.D. Wittrup, Biophysical properties of the clinical-stage antibody landscape, P Natl Acad Sci 114 (2017) 944.
[85] N.L. Dirks, B. Meibohm, Population pharmacokinetics of therapeutic monoclonal antibodies, Clin. Pharmacokinet. 49 (2010) 633–659.
[86] C.C. Michel, Transport of macromolecules through microvascular walls, Cardiovasc. Res. 32 (1996) 644–653.
[87] A.W. Stanton, W.E. Svensson, R.H. Mellor, A.M. Peters, J.R. Levick, P.S. Mortimer, Differences in lymph drainage between swollen and non-swollen regions in arms with breast-cancer-related lymphoedema, Clin. Sci. (Lond.) 101 (2001) 131–140.
[88] L. Zhao, P. Ji, Z. Li, P. Roy, C.G. Sahajwalla, The antibody drug absorption following subcutaneous or intramuscular administration and its mathematical description by coupling physiologically based absorption process with the conventional compartment pharmacokinetic model, J. Clin. Pharmacol. 53 (2013) 314–325.
[89] K. Haraya, T. Tachibana, J. Nezu, Quantitative prediction of therapeutic antibody pharmacokinetics after intravenous and subcutaneous injection in human, Drug Metab. Pharmacokinet. 32 (2017) 208–217.
[90] Y. Zheng, D.B. Tesar, L. Benincosa, H. Birnböck, C.A. Boswell, D. Bumbaca, K. J. Cowan, D.M. Danilenko, A.L. Daugherty, P.J. Fielder, H.P. Grimm, A. Joshi, N. Justies, G. Kolaitis, N. Lewin-Koh, J. Li, S. McVay, J. O'Mahony, M. Otteneder, M. Pantze, W.S. Putnam, Z.J. Qiu, J. Ruppel, T. Singer, O. Stauch, F.P. Theil, J. Visich, J. Yang, Y. Ying, L.A. Khawli, W.F. Richter, Minipig as a potential translatable model for monoclonal antibody pharmacokinetics after intravenous and subcutaneous administration, mAbs 4 (2012) 243–255.
[91] C.A. Boswell, D.B. Tesar, K. Mukhyala, F.P. Theil, P.J. Fielder, L.A. Khawli, Effects of charge on antibody tissue distribution and pharmacokinetics, Bioconjug. Chem. 21 (2010) 2153–2163.
[92] G. Thiagarajan, A. Semple, J.K. James, J.K. Cheung, M. Shameem, A comparison of biophysical characterization techniques in predicting monoclonal antibody stability, MAbs 8 (2016) 1088–1097.
[93] L. Xing, Y. Li, T. Li, Local concentrating, not shear stress, that may Lead to possible instability of protein molecules during syringe injection: a fluid dynamic study with two-phase flow model, PDA J. Pharm. Sci. Technol. 73 (2019) 260–275.